

Linear estimation of flux sensitivity to uncertainty in porous media

By **A. J. EVANS**¹, **C. P. CAULFIELD**^{1,2}
AND **ANDREW W. WOODS**¹

¹BP Institute, University of Cambridge, Madingley Rise, Madingley Road, Cambridge, CB3 0EZ, UK

²Department of Applied Mathematics & Theoretical Physics, Centre for Mathematical Sciences, University of Cambridge, Wilberforce Road, Cambridge CB3 0WA, UK

(Received February 2, 2015)

We derive an integral expression for the flux of a single phase fluid through a porous medium with prescribed boundary conditions. Taking variations with respect to the parameters of a given permeability model yields an integral expression for the sensitivity of the flux. We then extend the method to consider linear changes in permeability. This yields a linearised flux expression which is independent of changes in the pressure field that result from the changes in the permeability. For demonstration purposes, we first consider an idealised layered porous medium with a point source and point sink. We show how the effects of changes in permeability are affected by the position of the source and sink relative to the layered structure as well as the layer height and orientation of the layered structure. The results demonstrate that, even in a simple porous system, flux estimates are sensitive to the way in which the permeability is represented. We derive relationships between the statistical moments of the flux and of the permeability parameters which are modelled as random variables. This allows us to estimate the number of permeability parameters that should be varied in a fully nonlinear calculation to determine the variance of the flux. We demonstrate application of the methods to permeability fields generated through fast fourier transform and kriging methods. We show that the linear estimates for the variability in flux show good agreement with fully nonlinear calculations for sufficiently small standard deviations in the underlying permeability.

1. Introduction

Understanding the behaviour of fluids in subsurface rocks is important in a wide range of applications including hydrocarbon extraction, CO₂ sequestration and contaminant dispersal. As well as the need for accurate flow models, numerical solutions to these models need to be calculated on a reasonable timescale in order to be of use (Gerritsen & Durlofsky 2005). Flow in porous media is governed by rock pore geometry scales of the order of 0.01 – 1 mm whilst data collected through extracted rock cores and seismic imaging typically provide, at best, a 10 m resolution (Yilmaz 2001). Also, despite advances in computing resources, solving models with the large amounts of data needed to describe the flow geometry can become prohibitively difficult.

In order to progress, one can introduce effective media models which represent properties of the flow by specifying average property values on subdomains of the flow domain, an example of upscaling. Examples and critical reviews of upscaling within the fields of oil extraction and groundwater flow have been given by, among others, Desbarats (1992);

King et al (1995); Wen & Gómez-Hernández (1996); Christie (1996); Renard & de Marsily (1997); Chilés & Delfiner (1999); Farmer (2002); Wu, Efendiev & Hou (2002); Cushman, Bennethum & Hu (2002) and Fiori, Dagan & Jankovic (2013). Information is inevitably lost and uncertainty introduced when modelling the flow of fluid through the detailed rock structure in this way. Uncertainty is equivalent to a potential economic cost when attempting to extract or inject valuable fluid out of or into the rock (Jahn, Cook & Graham 2008). Furthermore, there is a considerable cost in acquiring further core and seismic data. As such, quantification of the level of uncertainty in a flow estimate can be of material financial importance.

A key physical property is the rock permeability which represents the ability of fluid to pass through the network of pores that make up the micro-structure of the rock. In the Darcy description of porous media flow,

$$\mathbf{u}^* = -\frac{k}{\mu} \nabla p^*, \quad (1.1)$$

permeability is parameterised as the spatially varying coefficient $k = k(\mathbf{x})$, defined as the ratio of the product of the Darcy velocity, \mathbf{u}^* , and the fluid viscosity, μ , to the pressure gradient ∇p^* applied across the porous medium. The scalar permeability k can be generalised to a symmetric matrix \mathbf{K} which represents anisotropic permeability where the eigenvalues of \mathbf{K} represent the scalar permeabilities (principal permeabilities) in the directions of anisotropy which are given by the eigenvectors of \mathbf{K} (Bear 1972). Uncertainty over the value of k (or the coefficients of \mathbf{K} in the anisotropic case) leads to uncertainty in the flow solution which is difficult to quantify without repeated calculations for many sampled values of permeability across the domain. Our aim is to gain a better understanding of the sensitivity of fluid flux to uncertainty in estimates of permeability whilst avoiding the need for computationally intensive models (e.g. Monte Carlo methods). We do this by finding the variations of an integral representation of the flux with respect to perturbations in the permeability.

Given poorly resolved data for the permeability, interpolation techniques are often used to construct an estimation for the permeability across the flow domain. A widely used example of linear interpolation in mining, hydrology and fossil fuel extraction is kriging. Kriging was first proposed by D. G. Krige (Krige 1951) and subsequently promoted and developed by G. Matheron (Matheron 1971). There are several forms of kriging including ‘simple’, ‘ordinary’ and ‘universal’ which each make different assumptions for the properties of the quantity of interest. For example, ‘ordinary’ kriging assumes that the function defining the correlation between two points is uniformly defined across the domain, and that the mean value is spatially constant, although freely determined.

In §2 we derive an integral expression for the flux of a single phase fluid through a porous medium with prescribed boundary conditions and permeability field. In §3 we present a method to calculate the dependence of the flux on variations in parameters of the permeability model. As an example we consider an idealised porous medium with a layered structure and isotropic permeability and discretise the permeability field by specifying spatially constant values for the permeability on discrete subdomains. We show that the model predictions are strongly influenced by the position of the source and sink relative to the layered structure as well as the height and orientation of the layered structure. We show that even in this simple scenario, the range of values calculated can be significant. In §4 we interpret the permeability as the sum of a spatially variable mean K_0 and a perturbation ϵK_1 which represents uncertainty within the data used to estimate K_0 . From this interpretation we obtain a leading order integral expression for the flux which depends upon the permeability and the leading order pressure field associated with

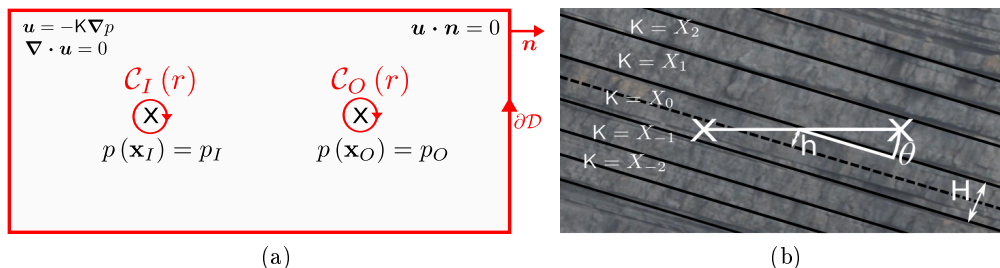


Figure 1: (a) Two dimensional schematic of a flow domain \mathcal{D} . Source/sink positions are shown by crosses and contours of $\partial\mathcal{S}$ ($\mathcal{C}_I(r)$, $\mathcal{C}_O(r)$) and $\partial\mathcal{D}$ the boundary of \mathcal{D}) are shown in red. (b) Schematic of source and sink positions, position parameters h and θ , and subdomains (boundaries marked in black) with assigned permeabilities X_i and layer height H .

the mean permeability K_0 . We define the discrete permeability parameters as random variables where the mean of each random variable corresponds to the value of K_0 on the corresponding subdomain of the flow domain. The variance of each random variable then corresponds to the local uncertainty in the estimate for the permeability. The discretisation of our permeability yields a direct expression for the variance of the total flux as a function of the variances of the random variables that represent the permeability. We compare these linear estimates to calculations of the nonlinear mean and variance of the flux calculated through sampling from probability distributions for the permeability. In §5 we allow for different mean permeability values across different layered subdomains to show how this change affects the results of our methods. In §6 we describe the generation of stochastic realisations of permeability fields and we develop the approach of §4 for application to these realisations of the permeability. In §7 and §8 we use ordinary kriging and a constrained optimisation approach respectively to interpolate the permeability from a surrogate truth model given by a realisation of a permeability field determined by fast fourier transform methods as described in §6. For each of the two interpolation methods we vary the correlation length scale of the interpolation scheme and estimate the values of the flux which result. Nonlinear and linear results are compared within §§6–8 to assess the validity of our linear methods to heterogeneous permeability fields. Finally, in §9 we draw our conclusions.

2. Flux expression

We consider a closed domain \mathcal{D} consisting of a porous medium with an input source located at \mathbf{x}_I and an output sink at \mathbf{x}_O each with prescribed pressure

$$p^*(\mathbf{x}_I) = p_I^*, \quad p^*(\mathbf{x}_O) = p_O^*, \quad (2.1a,b)$$

with $p_I^* > p_O^*$. We assume that Darcy's Law holds for an incompressible fluid with velocity \mathbf{u} , and so

$$\mathbf{u} = -K\nabla p, \quad \nabla \cdot \mathbf{u} = 0, \quad (2.2a,b)$$

where we have now non-dimensionalised with respect to the assumed constant fluid viscosity and where K is a symmetric matrix parameterisation of the in general anisotropic

permeability. We impose a no flow condition at the boundary of our domain, i.e.

$$\mathbf{u} \cdot \mathbf{n} = 0, \quad (2.3)$$

where \mathbf{n} is the outward facing normal vector to the domain boundary. The total flux Q can be written as a limiting integral around the source or the sink,

$$Q = - \lim_{r \rightarrow 0} \oint_{\mathcal{C}_I(r)} \mathbf{u} \cdot \mathbf{n} dS = \lim_{r \rightarrow 0} \oint_{\mathcal{C}_O(r)} \mathbf{u} \cdot \mathbf{n} dS, \quad (2.4)$$

where $\mathcal{C}_I(r)$ and $\mathcal{C}_O(r)$ are circles of radius r around the source and sink respectively (see figure 1a). Note that the normal vector \mathbf{n} here is pointing towards the source or sink to be consistent in orientation with the domain boundary normal. Using (2.1),

$$Q\Delta p = Q(p_I - p_O) = - \lim_{r \rightarrow 0} \left(\oint_{\mathcal{C}_I(r)} p(\mathbf{u} \cdot \mathbf{n}) dS + \oint_{\mathcal{C}_O(r)} p(\mathbf{u} \cdot \mathbf{n}) dS \right), \quad (2.5)$$

where p_I and p_O are the non-dimensionalised pressures at the source and sink. By noting (2.3) and then applying the divergence theorem followed by (2.2b),

$$Q\Delta p = - \lim_{r \rightarrow 0} \oint_{\partial\mathcal{S}} p(\mathbf{u} \cdot \mathbf{n}) dS = - \int_{\mathcal{D}} \nabla \cdot (p\mathbf{u}) dV = - \int_{\mathcal{D}} (\nabla p)^\top \mathbf{u} dV, \quad (2.6)$$

where $\partial\mathcal{S}$ is the union of the boundary of \mathcal{D} with \mathcal{C}_I and \mathcal{C}_O and $(\nabla p)^\top$ is the matrix transpose of ∇p . Finally, Darcy's Law yields

$$Q\Delta p = \int_{\mathcal{D}} (\nabla p)^\top \mathcal{K} \nabla p dV. \quad (2.7)$$

Note that (2.7) also holds for an infinite flow domain provided the fluid velocity decays sufficiently rapidly in the far field $|\mathbf{x}|^{d-1} \mathbf{u} \rightarrow \mathbf{0}$ as $|\mathbf{x}| \rightarrow \infty$ where $|\mathbf{x}|$ is the Euclidean distance from the origin and d is the spatial dimension of the flow domain. We note that in the case of a time dependent pressure change between the source and sink $\Delta p(t)$, the flux $Q(t)$ is given by $Q(t) = \Delta p(t) Q(t_0) / \Delta p(t_0)$ for any reference time t_0 . This is because the pressure gradients in (2.7) will scale with $\Delta p(t)$ for single phase flow. For multiple sources and/or multiple sinks the derivation above can be easily adapted to show that for source and sink outflow fluxes Q_i and pressures p_i , (2.7) becomes

$$\sum_i Q_i p_i = \int_{\mathcal{D}} (\nabla p)^\top \mathcal{K} \nabla p dV. \quad (2.8)$$

Note that $Q_i < 0$ for flow into a sink.

3. Parameter sensitivity

The permeability $\mathcal{K} = \mathcal{K}(\mathbf{x}, \boldsymbol{\alpha})$ is, in general, a function of space \mathbf{x} and parameters $\boldsymbol{\alpha} = (\alpha_1, \alpha_2, \dots, \alpha_n)$. The partial derivative of the flux with respect to parameter α_i gives the dependence of the flux to variations in the parameter α_i i.e.

$$\frac{\partial Q}{\partial \alpha_i} = \frac{1}{\Delta p} \int_{\mathcal{D}} (\nabla p)^\top \frac{\partial \mathcal{K}}{\partial \alpha_i} \nabla p dV + \frac{2}{\Delta p} \int_{\mathcal{D}} (\nabla p)^\top \mathcal{K} \frac{\partial (\nabla p)}{\partial \alpha_i} dV, \quad (3.1)$$

using (2.7) with the second term resulting from the symmetry of the integrand. Darcy's law (2.2a), the divergence theorem and (2.2b) yield

$$\int_{\mathcal{D}} (\nabla p)^\top \mathcal{K} \frac{\partial (\nabla p)}{\partial \alpha_i} dV = \int_{\mathcal{D}} \mathbf{u}^\top \nabla \left(\frac{\partial p}{\partial \alpha_i} \right) dV = \lim_{r \rightarrow 0} \int_{\partial\mathcal{S}} (\mathbf{u} \cdot \mathbf{n}) \left(\frac{\partial p}{\partial \alpha_i} \right) dS = 0, \quad (3.2)$$

as $\mathbf{u} \cdot \mathbf{n} = 0$ on the boundary of \mathcal{D} and the pressure is prescribed and constant ($\partial p / \partial \alpha_i = 0$) at the source and the sink. Therefore (3.1) becomes

$$\frac{\partial Q}{\partial \alpha_i} = \frac{1}{\Delta p} \int_{\mathcal{D}} (\nabla p)^\top \frac{\partial \mathcal{K}}{\partial \alpha_i} \nabla p dV. \quad (3.3)$$

Equation (3.3) can be used to quantify the sensitivity of the flux to changes in parameters within a given model for the permeability provided $\partial \mathcal{K} / \partial \alpha_i$ can be computed. Examples of such parameters include values of permeabilities at points in space or correlation length scales used within interpolation methods. We will discuss correlation length scales within interpolation methods in more detail in §7 and §8. Use of (3.3) does not require repeated calculation of solutions to the flow equations (2.1), (2.2) and (2.3) for many realisations of a varying permeability field.

A model for the permeability which is widely used (see, for example, Wen & Gómez-Hernández (1996)) involves defining the permeability to be spatially constant within finite size subdomains of the flow domain. The parameters for this spatially discrete permeability field are the values for the permeability on each subdomain, as shown schematically in figure 1b. The flux is then given by a linear combination of the parameters X_i which represent the permeability. We denote by X_i the spatially constant value of the permeability in subdomain $\mathcal{D}_i \subseteq \mathcal{D}$ as shown in figure 1b. Equation (2.7) yields

$$Q = \frac{1}{\Delta p} \int_{\mathcal{D}} (\nabla p)^\top \mathcal{K} \nabla p dV = \left(\frac{1}{\Delta p} \int_{\mathcal{D}_i} |\nabla p|^2 dS \right) X_i \equiv a_i X_i, \quad (3.4)$$

using the Einstein summation convention. With the permeability described by the parameters X_i in this way, equation (3.3) becomes

$$\frac{\partial Q}{\partial X_i} = a_i. \quad (3.5)$$

Thus we see that the integrals a_i defined in (3.4) give the magnitude of the sensitivity of the flux to variations in the corresponding permeability parameters.

In order to demonstrate an application of the above results we consider an idealised porous medium. Specifically, we consider a layered system with each of the layer permeability parameters X_i set to be equal. That is, the permeability \mathcal{K} is modelled as spatially constant and isotropic across the entire domain. This is representative of a layered system where the rock properties in individual layers are similar though their deposition is associated with different geological events. We show that the resulting flux derivatives are sensitive to the position of the source and the sink relative to the layer boundaries.

We scale our domain by the distance between the source and sink locations d which we set to be 1. Our flow domain is a 2 by 2 square. We set each of the layer heights as a constant H . We define the positions of the source and sink by describing the line joining their locations with two parameters: h the displacement of the midpoint of the straight line connecting the source to the sink from the centre of the layer containing this midpoint; and θ the angle between the straight line connecting the source to the sink and the layer boundaries, as shown in figure 1b. Due to the symmetry of the permeability field, $h/H \in [-0.5, 0.5]$ and $\theta \in [0, \pi/2]$ describe the range of unique source and sink positions relative to the layered structure. We plot flow streamlines with overlaid layer boundaries shown in black for: $h/H = 0, \theta = 0, H/d = 0.4$ (figure 2a) and $h/H = 0.5, \theta = 0, H/d = 0.4$ (figure 2b).

For a layer angle of $\theta = 0$ and for $H/d = 0.4$, figure 2c shows the variation with h/H of a_i for the layer in which the source and sink are located (layer 0) and the two adjacent layers (layers -1 and 1). We see that the a_i are sensitive to the position of the source

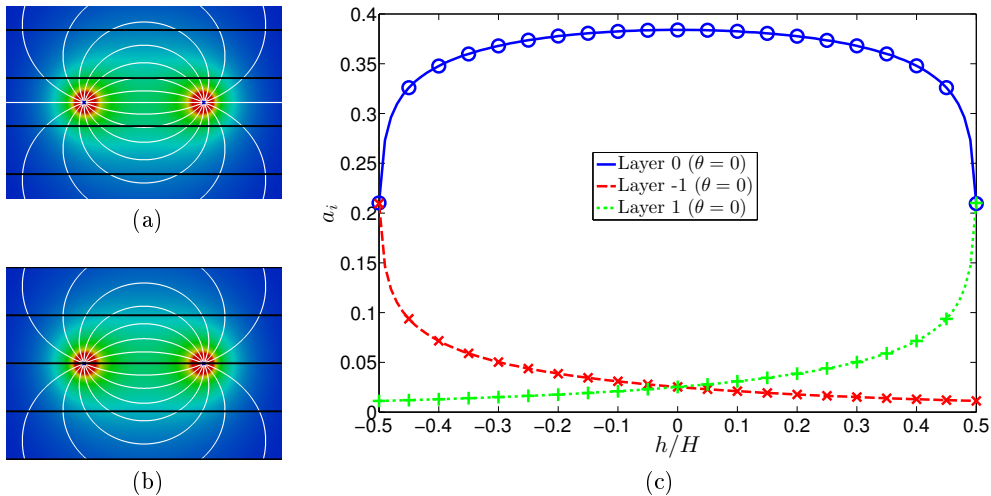


Figure 2: Flow streamlines with overlaid layer boundaries shown in black with: (a) $h = 0, \theta = 0, H/d = 0.4$, (b) $h/H = 0.5, \theta = 0, H/d = 0.4$. (c) Variation with sink position h/H of a_i (defined in (3.4)) for the central three layers with $H/d = 0.4$ and layer orientation $\theta = 0$.

and the sink relative to the layered structure. The central layer (layer 0) has the largest value across the full range of values for h which is to be expected as layer 0 contains the source and the sink for this value of θ (see figures 2a and 2b) and thus contains the largest pressure gradients due to the uniformity of the mean permeability K_0 . The value of a_0 is maximised when $h/H = 0$ as here the source and the sink are in the centre of layer 0 (see figure 2a).

We plot flow streamlines with overlaid layer boundaries in black for: $h = 0, \theta = \pi/6, H/d = 0.4$ (figure 3a) and $h = 0, \theta = \pi/6, H/d = 0.1$ (figure 3b). In figure 3c we plot a_i against layer number for layer heights given by $H/d = 0.1$ (green), $H/d = 0.4$ (black) and $H/d = 1.6$ (red). The values are averaged across 101 incremental values of $h/H \in [-0.5, 0.5]$ and across 101 values of $\theta \in [0, \pi/2]$. As the ratio of layer height to source/sink spacing H/d decreases, the number of layers spanning the flow domain increases. The total number of layers for $H/d = 0.1$ is fifty-seven with the central twenty-one plotted; the values of the a_i outside this range continue decreasing to zero in either direction.

For $H/d = 1.6$ the distribution of the a_i is unimodal since the source and the sink both lie within layer 0 for a large range of values in $(h/H, \theta) \in [-0.5, 0.5] \times [0, \pi/2]$ due to the large layer height, H , relative to the source/sink spacing, d . However, for $H/d = 0.4$ and 0.1 , the distribution of the a_i becomes bimodal when averaged across $\theta \in [0, \pi/2]$. Due to the small layer height relative to the source/sink spacing, the source and the sink are located in many different layers as θ is varied (see figure 3b). This qualitative change in distribution appears to occur close to $H/d = 0.4$.

Our method can be used to calculate the number of parameters which should be varied within a more computationally intensive nonlinear model. We consider the “proportional

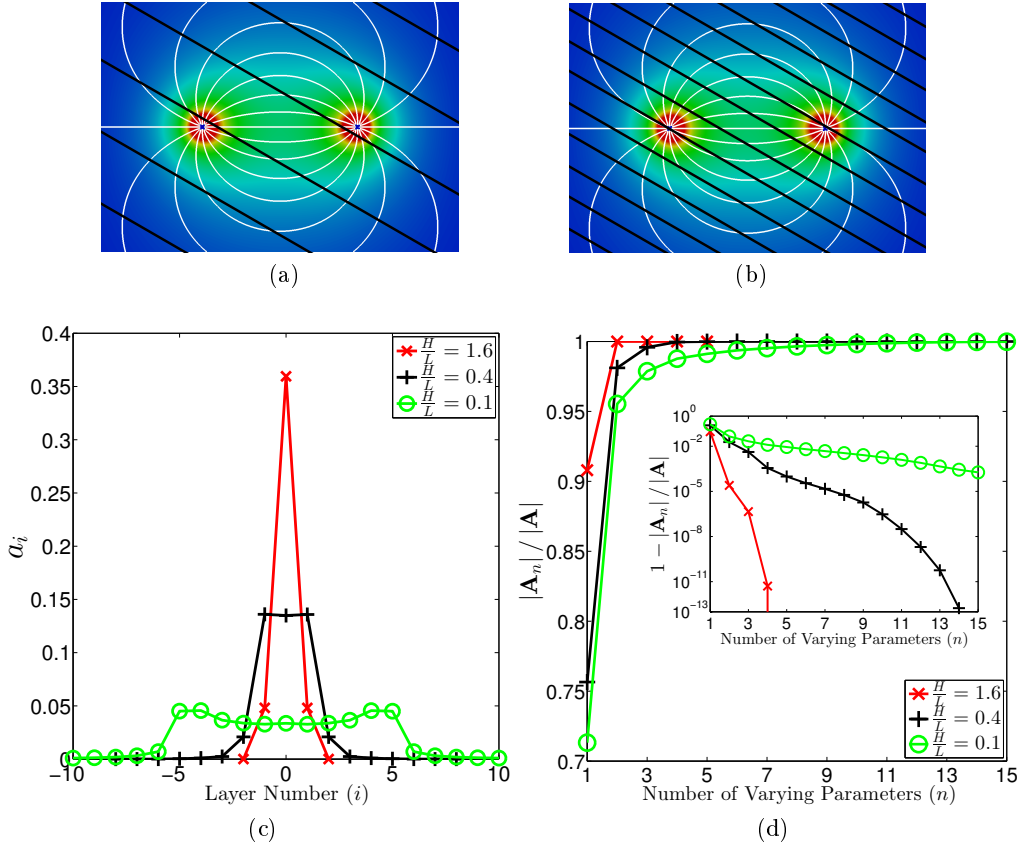


Figure 3: (a),(b) Flow streamlines with overlaid layer boundaries shown in black with: (a) $h = 0, \theta = \pi/6, H/d = 0.4$, (b) $h = 0, \theta = \pi/6, H/d = 0.1$. (c) Variation between layers of a_i averaged across 101 values of position parameter $h/H \in [-0.5, 0.5]$ and 101 values of layer angle $\theta \in [0, \pi/2]$ for three different layer heights $H/d = 0.1$ (green with circles), $H/d = 0.4$ (black with upright crosses) and $H/d = 1.6$ (red with slanted crosses). (d) The dependence of the proportional flux variation, $|\mathbf{A}_n|/|\mathbf{A}|$ defined in (3.6), on the number of parameters varied when averaged across 101 values of $h/H \in [-0.5, 0.5]$ and 101 values of $\theta \in [0, \pi/2]$ for $H/d = 0.1$ (green with circles), $H/d = 0.4$ (black with upright crosses) and $H/d = 1.6$ (red with slanted crosses).

flux variation" $|\mathbf{A}_n|/|\mathbf{A}|$ defined as

$$\frac{|\mathbf{A}_n|}{|\mathbf{A}|} = \frac{\left(\sum_{i=1}^n A_i^2\right)^{\frac{1}{2}}}{\left(\sum_{i=1}^N A_i^2\right)^{\frac{1}{2}}} \quad A_1 \geq A_2 \geq A_3 \dots \quad (3.6)$$

where $\mathbf{A} = (A_1, A_2, \dots)$ is the ordered vector of coefficients a_i and N is the total number of layers. $|\mathbf{A}_n|/|\mathbf{A}|$ is the ratio of the variation in the flux that results from varying the n most significant of the parameters X_i to the flux variation resulting from varying the full set of X_i . Figure 3d plots $|\mathbf{A}_n|/|\mathbf{A}|$ as a function of n for $H/d = 0.1, 0.4, 1.6$ when averaged across h and θ . Figure 3d shows that for $H/d = 1.6$, variation in the permeability value of the most dominant layer accounts for a very large proportion of

the total variation in flux that results from varying all of the parameters, while decreasing H/d requires more and more layers to account for the same proportion of the total flux variation.

4. Linearised flux sensitivity

We can extend our approach to gain a quantitative estimate of the variance of the flux in the case of small perturbations of the permeability. We write the permeability as the sum of a fixed K_0 and a small perturbation ϵK_1 where $\epsilon \ll 1$. ϵK_1 represents the uncertainty in the mean permeability K_0 estimated from available data. We similarly expand the fluid pressure, velocity and flux

$$K = K_0 + \epsilon K_1, \quad p = p_0 + \delta_p p_1 + \delta_p^2 p_2 \dots, \quad (4.1a,b)$$

$$\mathbf{u} = \mathbf{u}_0 + \delta_u \mathbf{u}_1 + \delta_u^2 \mathbf{u}_2 \dots, \quad Q = Q_0 + \delta_q Q_1 + \delta_q^2 Q_2 \dots, \quad (4.1c,d)$$

where $\epsilon, \delta_u, \delta_q, \delta_p \ll 1$. We include second order terms to find the sign of the second order flux correction. The no-flow condition (2.3) applies to both \mathbf{u}_0 and \mathbf{u}_1 on $\partial\mathcal{D}$. The leading order pressure p_0 has boundary conditions at the source and sink given by (2.1), so $p_i = 0$ at both the source and the sink for all $i \geq 1$.

Darcy's Law (2.2a) becomes to first order

$$\mathbf{u}_0 + \delta_u \mathbf{u}_1 = -K_0 \nabla p_0 - \epsilon K_1 \nabla p_0 - \delta_p K_0 \nabla p_1, \quad (4.2)$$

while (2.7) yields to second order

$$\begin{aligned} (Q_0 + \delta_q Q_1 + \delta_q^2 Q_2) \Delta p &= \int_{\mathcal{D}} (\nabla p_0)^\top K_0 \nabla p_0 \, dV \\ &\quad + \int_{\mathcal{D}} \epsilon (\nabla p_0)^\top K_1 \nabla p_0 + 2\delta_p (\nabla p_0)^\top K_0 \nabla p_1 \, dV \\ &\quad + \int_{\mathcal{D}} \delta_p^2 (\nabla p_1)^\top K_0 \nabla p_1 + 2\epsilon\delta_p (\nabla p_0)^\top K_1 \nabla p_1 + 2\delta_p^2 (\nabla p_0)^\top K_0 \nabla p_2 \, dV. \end{aligned} \quad (4.3)$$

By definition

$$Q_0 \Delta p = \int_{\mathcal{D}} (\nabla p_0)^\top K_0 \nabla p_0 \, dV, \quad (4.4)$$

and by making the natural scaling assumption, $\delta_q = \delta_p = \epsilon$, and using (4.2), we obtain

$$Q_1 \Delta p = \int_{\mathcal{D}} (\nabla p_0)^\top K_1 \nabla p_0 \, dV - 2 \int_{\mathcal{D}} \mathbf{u}_0^\top \nabla p_1 \, dV, \quad (4.5)$$

$$Q_2 \Delta p = - \int_{\mathcal{D}} (\nabla p_1)^\top K_0 \nabla p_1 \, dV - 2 \int_{\mathcal{D}} \mathbf{u}_1^\top \nabla p_1 + \mathbf{u}_0^\top \nabla p_2 \, dV. \quad (4.6)$$

We note that the natural scaling assumption $\delta_q = \delta_p = \epsilon$ can be shown to be the only non-trivial balance between the terms of (4.2) and (4.3). Finally, with r and $\partial\mathcal{S}$ defined as in §2, the divergence theorem yields

$$\int_{\mathcal{D}} \mathbf{u}_0^\top \nabla p_1 \, dV = \lim_{r \rightarrow 0} \oint_{\partial\mathcal{S}} (\mathbf{u}_0 \cdot \mathbf{n}) p_1 \, dS = 0, \quad (4.7)$$

$$\int_{\mathcal{D}} \mathbf{u}_1^\top \nabla p_1 + \mathbf{u}_0^\top \nabla p_2 \, dV = \lim_{r \rightarrow 0} \oint_{\partial\mathcal{S}} (\mathbf{u}_1 \cdot \mathbf{n}) p_1 + (\mathbf{u}_0 \cdot \mathbf{n}) p_2 \, dS = 0, \quad (4.8)$$

as $p_1 = p_2 = 0$ at the source and the sink and $\mathbf{u}_0 \cdot \mathbf{n} = \mathbf{u}_1 \cdot \mathbf{n} = 0$ on the boundary of

\mathcal{D} . Dropping higher order terms we obtain expressions for the leading order change and second order correction in flux due to the perturbation in permeability

$$Q_1 = \frac{1}{\Delta p} \int_{\mathcal{D}} (\nabla p_0)^\top K_1 \nabla p_0 dV, \quad Q_2 = -\frac{1}{\Delta p} \int_{\mathcal{D}} (\nabla p_1)^\top K_0 \nabla p_1 dV. \quad (4.9a,b)$$

We note that (4.9a) is independent of the pressure perturbation ϵp_1 , a property we shall exploit in a similar manner to §3. Combining (4.4) and (4.9a) we see that the total flux Q to first order in ϵ is given by

$$Q = \frac{1}{\Delta p} \int_{\mathcal{D}} (\nabla p_0)^\top K \nabla p_0 dV + O(\epsilon^2). \quad (4.10)$$

The key difference between (4.10) and the exact expression for the flux (2.7) is that (4.10) does not require the recalculation of the full pressure field p for a change in the permeability, but rather depends only on the leading order pressure p_0 . We also note that (4.9b) is negative definite and so the first order in ϵ approximation of the flux is at least a local upper bound for the full nonlinear flux.

We now consider modelling the permeability K as a random field. We can use (4.10) to calculate statistical moments of the flux resulting from a probability distribution for the permeability. We consider the parameters X_i from §3 to be independent random variables with constant means μ_i and variances σ_i^2 where parameter X_i represents the value of the permeability on subdomain \mathcal{D}_i . As in §3 it follows from (4.10) that

$$Q \simeq \frac{1}{\Delta p} \int_{\mathcal{D}} (\nabla p_0)^\top K \nabla p_0 dV = \left(\frac{1}{\Delta p} \int_{\mathcal{D}_i} |\nabla p_0|^2 dS \right) X_i \equiv a_{0i} X_i, \quad (4.11)$$

where we have once again used the Einstein summation convention. Hence, the expected value and variance σ_Q^2 of Q are given by, to first order in ϵ ,

$$\mathbb{E}(Q) = a_{0i} \mu_i, \quad \sigma_Q^2 = a_{0i}^2 \sigma_i^2. \quad (4.12a,b)$$

It is important to emphasise that the coefficients a_{0i}^2 are independent of the distribution of the permeability.

We shall now compare these linear estimates to the nonlinear mean and variance of the flux. We consider each of the permeabilities X_i to be log-normally distributed with constant and uniform mean K_0 and standard deviation $\sigma_K \in [0, 1]$. We compute the pressure field p and hence the flux Q for each sample set of values for the X_i drawn at incremental percentiles of the assigned log-normal distributions. From these sample flux values we then calculate the nonlinear estimates of the mean and standard deviation for the flux. The sampling is performed using this systematic method in order to resolve the tails of the permeability distributions with the limited number of samples taken. The number of samples is limited by the computational expense of the associated pressure calculations. We also calculate the linear estimates for the mean and standard deviation of the flux as described by (4.11) and (4.12), which only uses the flux value corresponding to $X_i = K_0$ for all i . For this example, we consider the same layered system as described in §3 with the layer height fixed at $H/d = 0.4$ and the source and sink positions relative to the layered structure determined by $h/H = \theta = 0$. For illustration, we consider two simple examples. In example C1 we vary the permeability of the central layer alone, and in example C3 we vary the permeability of the central three layers. All other parameters X_i are held constant and equal to K_0 . Without loss of generality, we set $K_0 = 1$.

Figures 4a and 4b show the comparison between linear estimates, shown by black lines, and nonlinear calculations, shown by red lines, for the mean flux $\mathbb{E}(Q)$ and the standard deviation of the flux σ_Q normalised by $\mathbb{E}(Q)$ and as a fraction of the standard deviation of the permeability σ_K . In each figure results derived from example C1 are shown by

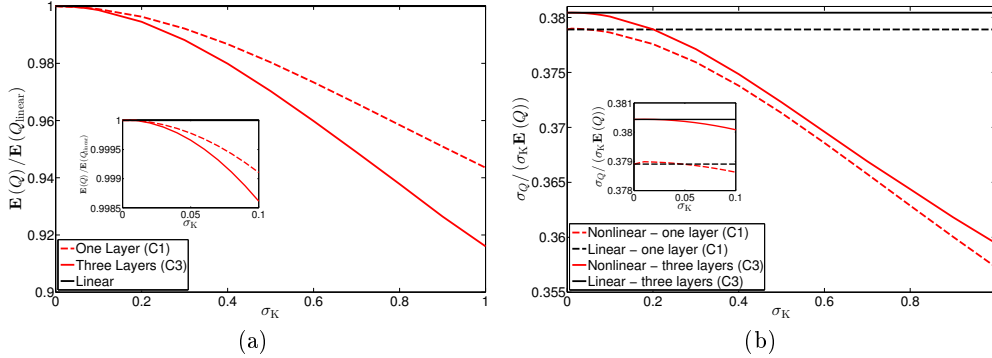


Figure 4: Comparison between linear estimates (black horizontal lines) and nonlinear calculations (red lines) for (a) the mean flux $\mathbb{E}(Q)$ and (b) the standard deviation of the flux σ_Q normalised by the mean flux $\mathbb{E}(Q)$ as a fraction of the standard deviation of the permeability σ_K . Results derived from example C1 (allowing one layer to vary) and example C3 (allowing three layers to vary) are shown by dashed lines and solid lines using 1000 and 64000 flux calculations respectively. Insets show behaviour for $\sigma_K \in [0, 0.1]$.

dashed lines and example C3 by solid lines. For example C1 we calculated the flux for 1000 permeability values in this layer, while for example C3 we calculated the flux for $40^3 = 64000$ permeability fields, i.e. 40 independent permeability values per layer varied. These sample sizes balance the need for adequate statistical convergence of the nonlinear estimates with the limitations imposed by the computation time required for a large number of pressure calculations. The linear estimates for the mean flux in examples C1 and C3 are equal (figure 4a) as the mean value of the permeability perturbations are zero in each of the varied layers. As expected, the linear and nonlinear results converge as the standard deviation of the permeability values σ_K tends to zero and the linear expected value for the flux is larger than the corresponding nonlinear values for all values of σ_K . As σ_K approaches the size of the base permeability, $K_0 = 1$, the linear estimate becomes invalid. However in the three layer example C3 the maximum difference between the linear and nonlinear estimates for the mean and normalised standard deviation of the flux is around 9% and 6% of the nonlinear mean and standard deviation respectively. It should be noted that the difference between the linear and nonlinear estimates increases between example C1 and example C3. The value of $|\mathbf{A}_n|/|\mathbf{A}|$ in the central layer (i.e. layer 0) is 0.757 and the value in the central three layers (layers -1,0,1) is 0.996 (see figure 3d) suggesting example C3 captures almost all of the nonlinear variation in flux. It is worth emphasising that the linear estimate required only one calculation of the pressure field compared with the 1000 and 64000 pressure calculations required for adequately converged nonlinear results.

5. Non-uniform mean permeabilities

In §3 and §4 we demonstrated the respective results for a uniform mean permeability $K_0 = 1$. We now consider the case where the mean value varies from layer to layer. We set the layer height to be $H = 0.4$. As a canonical example we change the value of K_0 for two neighbouring layers so as to see the effects this has on the sensitivity of the flux to these layers and to the surrounding layers. We set one layer to have mean permeability $K_{0,0} = 0.1$ (layer 0) and a neighbouring layer to have mean permeability

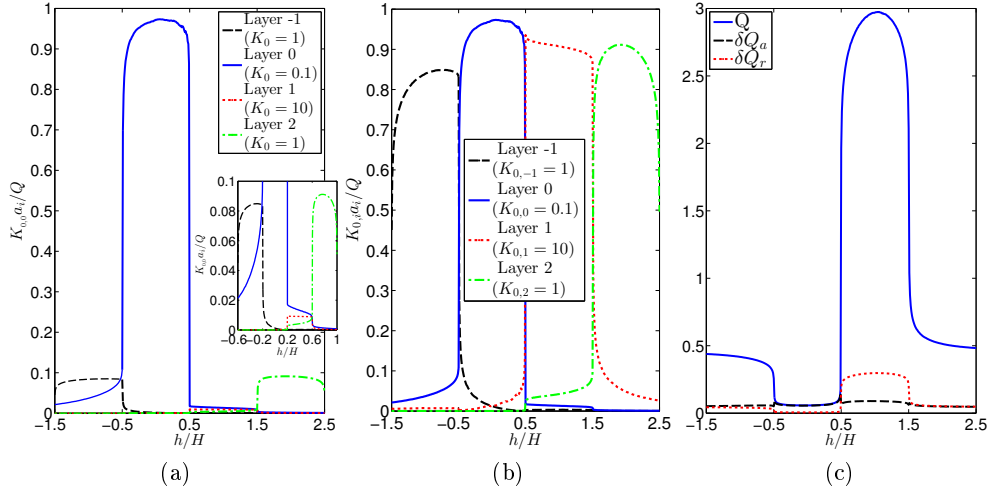


Figure 5: (a) Plot of flux sensitivities $K_{0,0}a_i$ normalised by flux Q for a constant change in permeability across layers. Inset shows values for range $K_{0,0}a_i/Q \in [0, 0.1]$. (b) Plot of flux sensitivities $K_{0,i}a_i$ normalised by flux Q for a change in permeability which is proportional to the mean permeability in each layer. Values plotted for four layers with varying mean permeabilities $K_{0,i}$ as shown in the legend. (c) Value of flux Q (shown by blue full line) and linear flux changes $\delta Q_a, \delta Q_r$ for constant permeability changes and permeability changes proportional to the mean layer permeabilities respectively (shown as black dashed and red dotted lines respectively). Values plotted as functions of source/sink position h/H as shown in figure 1b.

$K_{0,1} = 10$ (layer 1). All other layers continue to have $K_{0,i} = 1$. With nonuniform mean permeabilities we may consider changes in permeability which are equal in absolute size across layers or which scale with the mean permeability of each layer. For equal changes, (3.4) and (3.5) give the corresponding sensitivities of the flux to changes in permeability. For changes in permeability which scale with the mean we scale (3.4) and (3.5) by the mean permeabilities $K_{0,i}$ of each layer, i.e.

$$K_{0,i} \frac{\partial Q}{\partial X_i} = \frac{K_{0,i}}{\Delta p} \int_{\mathcal{D}_i} |\nabla p|^2 dS = K_{0,i} a_i, \quad (5.1)$$

where $K_{0,i}$ is the mean permeability of layer i . Equation (5.1) is equivalent to (3.4) and (3.5) for $K_0 = 1$. Figures 5a and 5b plot the values of $K_{0,0}a_i/Q$ and $K_{0,i}a_i/Q$ respectively for the two altered layers (layers 0 and 1) and the two neighbouring layers (layers -1 and 2). These values are plotted as functions of source and sink position $h/H \in [-1.5, 2.5]$ as defined in §3 and shown in figure 1b. This range of values corresponds to the source and sink within each of the four layers in turn.

The largest value of $K_{0,0}a_i/Q$ for all i occurs for layer 0 when the source and sink are within this layer. By contrast the values of $K_{0,0}a_1/Q$ are considerably smaller. This difference in values is because for changes in permeability which do not scale with the mean value, the relative size of the fluctuation is larger for the low permeability layer (layer 0) and hence the flux is more sensitive to this layer. Indeed, as highlighted in the inset plot within figure 5a, $K_{0,0}a_0/Q$ remains larger than $K_{0,0}a_1/Q$ even when the source and sink are within layer 1 ($h/H \in [0.5, 1.5]$). From figure 5b we note that the largest value of $K_{0,i}a_i$ for each value of h/H corresponds to the layer containing the source and

the sink and that the maximum value attained by each of the $K_{0,i}a_i$ is approximately equal for each layer. That is, when the permeability fluctuations scale with the mean value, the flux is most sensitive to the layer containing the source and sink and we are in a similar regime to the uniform mean value case $K_0 = 1$ from §3 and §4.

Figure 5c shows plots of the flux Q and the value of the absolute and relative changes in flux defined as

$$\delta Q_a = 0.1 \sum_i a_i, \quad \delta Q_r = 0.1 \sum_i K_{0,i}a_i, \quad (5.2a,b)$$

which correspond to the linear change in flux which results from changes in permeability which are constant across different layers or that scale with the mean permeability of each layer. We see that δQ_a is approximately constant as a function of source and sink position h/H . δQ_a is approximately equal to Q for $h/H \in [-0.5, 0.5]$ where the source and sink are within layer 0. This is because the change in permeability is here chosen as equal to 0.1 which is equal to $K_{0,0}$, the mean permeability of layer 0. By contrast δQ_r is by definition equal to $0.1Q$ and so the percentage or relative change in flux is constant across the range of source and sink positions as alluded to in figure 5b. We would expect our linear estimates to be least accurate for $h/H \in [-0.5, 0.5]$ in the case where the changes in permeability are taken to be constant across layers (where δQ_a is the linear change in flux). This is because the change in permeability is comparable in size to the mean permeability in the layer containing the highest pressure gradients.

6. Stochastic simulation

Stochastic simulations can be obtained in a large range of ways including matrix decomposition techniques (Davis 1987), moving average (Black & Freyberg 1990), nearest neighbour (King & Smith 1988), spectral methods (Borgman, Taheri & Hagan 1984) and turning bands (Mantoglou & Wilson 1982). An elegant method is proposed by Dietrich & Newsam (1993) which uses a fast fourier transform method to generate a gaussian simulation with a controllable correlation length scale. We have used this last method to generate the permeability field shown in figure 6a. We have chosen a correlation length scale of 0.4 for this simulation with the domain a 4 by 4 square. This simulation provides a more realistic example of a heterogeneous permeability field than those described in §§3–5 and allows us to explore the extent to which the techniques developed in this paper can be applied to such fields. Due to the stochastic nature of this technique, there is no analytic expression for the derivative of the flux with respect to parameters of the model, for example the correlation length scale prescribed. Hence we cannot use (3.3) directly. However, given multiple realisations of the permeability field, we can apply the linear method from §4, in particular (4.10), to estimate the associated values of the flux. That is, we calculate the pressure field p_0 for a chosen reference permeability K_0 and then use (4.10) to calculate the flux Q for a new permeability field K . This linear method can be applied to any sample set of permeability fields independent of the technique used to generate them if the change in permeability away from the reference permeability is small by comparison to the reference permeability.

We will now apply the linear method from §4 for sample sets of realisations of the permeability field produced by the methods of Dietrich & Newsam (1993). The direct output from this method is a field of values normally distributed about zero. In order to produce a positive permeability field one must scale and translate these values. For this example we apply an exponential transformation to the generated fields to produce permeability fields with values given by a log-normal distribution. We choose the scale

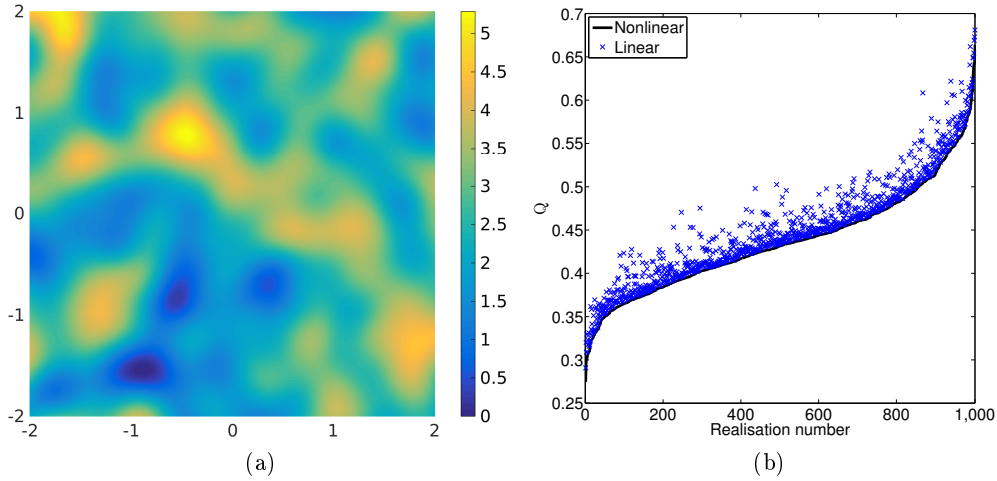


Figure 6: (a) Permeability field generated using a fast fourier transform method as proposed by Dietrich & Newsam (1993), with correlation length $L = 0.4$. (b) Plot of nonlinear flux calculations (shown by black line) and linear flux estimates (shown by blue crosses) for each of 1000 stochastically generated realisations of permeability with $L = 0.4, \sigma_K = 0.25$. Data ordered by the value of the nonlinear flux.

parameters so that the resulting fields each have mean value equal to 1 and have standard deviations which we will prescribe. Using this algorithm we have generated 16 sample sets each with 1000 permeability fields. Across these 16 sample sets we vary the correlation length scale L and the standard deviation σ_K of the permeability fields. We use four values for each with $L = 0.2, 0.4, 0.8, 1.6$ and $\sigma_K = 0.25, 0.5, 0.75, 1.0$. Each sample set of 1000 permeabilities has a unique pair of values for L and σ_K . We can then assess how the mismatch between linear and nonlinear estimates changes as the standard deviation of the permeability varies for each value of correlation length scale. According to (4.10) we expect differences between the linear and nonlinear estimates for the mean flux to be of order σ_K^2 as a fraction of the nonlinear estimate for the mean flux.

Figure 6b shows the values of the nonlinear flux and linear estimates of the flux for each of the 1000 permeability realisations with $L = 0.4, \sigma_K = 0.25$. The values are ordered so that the nonlinear values are monotonically increasing. The nonlinear values are calculated by explicitly solving for the pressure field for each realisation of the permeability. For the linear estimates we calculate the average value of the permeability across the 1000 samples at each point in the flow domain. We then calculate the pressure p_0 for this average permeability field and use (4.10) to estimate the flux with the permeability K given by each of the 1000 realisations in turn. We see that there is some scatter in the linear estimates and that they are all greater than the nonlinear values. The latter characteristic is consistent with the fact that the second order error term (4.9b) for the flux is negative. Physically this is because the linear estimate implicitly finds the arithmetic mean of the permeability fluctuations along a given flow streamline. However, the nonlinear flux value results from a combination of geometric and arithmetic averaging of permeabilities. As the geometric average is always smaller than or equal to the arithmetic mean, the linear estimate is always an upper bound. In figure 7a we show the percentage difference between the linear estimates and the exact nonlinear flux as a function of the nonlinear flux. The mean nonlinear flux is 0.436. We see that most of the flux values lie

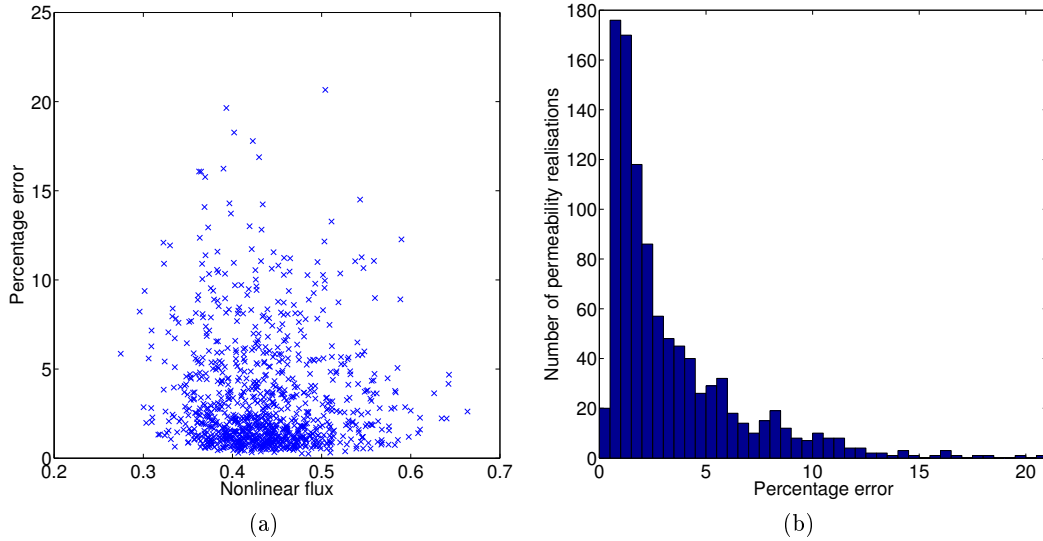


Figure 7: (a) Plot of percentage error for the 1000 linear estimates for the flux compared to the corresponding nonlinear flux calculation as a function of nonlinear flux with $L = 0.4$, $\sigma_K = 0.25$. (b) Histogram of percentage error for the 1000 linear estimates for the flux with $L = 0.4$, $\sigma_K = 0.25$ and with bin size equal to 0.5%.

between 0.35 and 0.51 with many of the percentage errors significantly below 5%. The maximum error is about 21%. Figure 7b shows a histogram of the percentage errors with bin size equal to 0.5%. We see that the majority of the error values do indeed lie below 5% with a peak between 0.5% and 1.5%.

For each of the 16 sets of 1000 permeability realisations we have nonlinearly calculated the mean and standard deviation of the flux. We have then linearly estimated the mean and standard deviation of the flux through use of (4.10). In figures 8a, 8b and 8c we plot the values of the mean flux $\mathbb{E}(Q)$; the standard deviation of the flux σ_Q and the ratio $\sigma_Q/\mathbb{E}(Q)$ of the mean and standard deviation of the flux as functions of normalised permeability standard deviation $\sigma_K/\mathbb{E}(K)$. Figure 8a shows that the nonlinearly calculated mean flux decreases as the variability in the permeability fields increases. This is consistent with the interpretation of the nonlinear flux being a combination of the geometric and arithmetic mean of the permeability fluctuations. In contrast the linear estimates for the mean flux do not change by a significant amount as the standard deviation of the permeability σ_K is increased. In figure 8b we see that the nonlinear values and linear estimates for the standard deviation of the flux again diverge for large σ_K with the linear estimates maintaining a linear trend with respect to σ_K . Figure 8c illustrates remarkably good agreement between nonlinear and linear estimates for the ratio $\sigma_Q/\mathbb{E}(Q)$. Across figures 8a, 8b and 8c we see that the nonlinear values of the mean flux $\mathbb{E}(Q)$; the standard deviation of the flux σ_Q and the ratio $\sigma_Q/\mathbb{E}(Q)$ all increase as the correlation length scale increases. This trend is not consistently captured by the linear estimates.

In figures 9a and 9b we plot the percentage differences between exact nonlinear values and linear estimates for the mean flux $\mathbb{E}(Q)$ and standard deviation of the flux σ_Q respectively. Values are plotted as functions of permeability standard deviation σ_K and the four lines in each figure correspond to different values of correlation length scale L . As expected, we see that the difference between the nonlinear and linear estimates increases

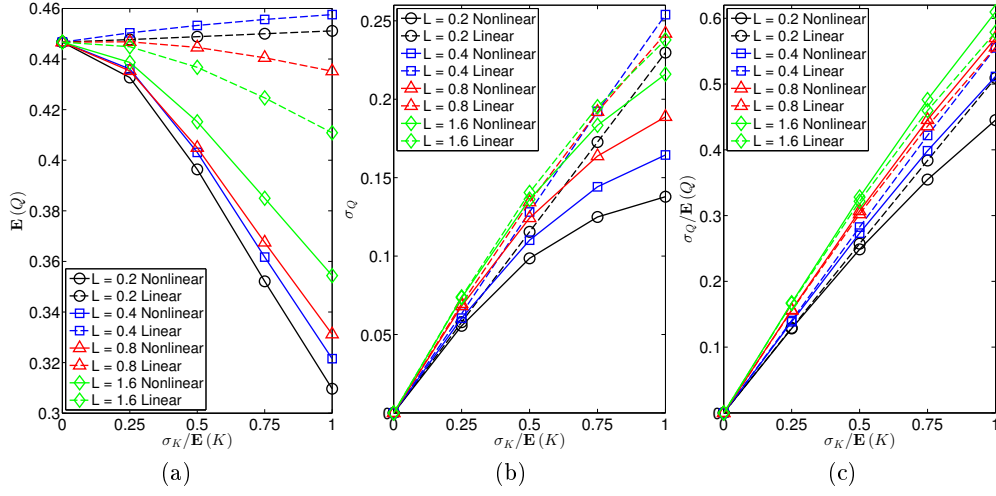


Figure 8: Plots of nonlinear and linear estimates for (a) the mean flux $\mathbb{E}(Q)$; (b) the standard deviation of the flux σ_Q and (c) the ratio $\sigma_Q/\mathbb{E}(Q)$ of the mean and standard deviation of the flux as functions of normalised permeability standard deviation $\sigma_K/\mathbb{E}(K)$. Values plotted for correlation length scales $L = 0.2$ (black with circles), $L = 0.4$ (blue with squares), $L = 0.8$ (red with triangles) and $L = 1.6$ (green with diamonds). Nonlinear estimates shown by full lines and linear estimates shown by dashed lines.

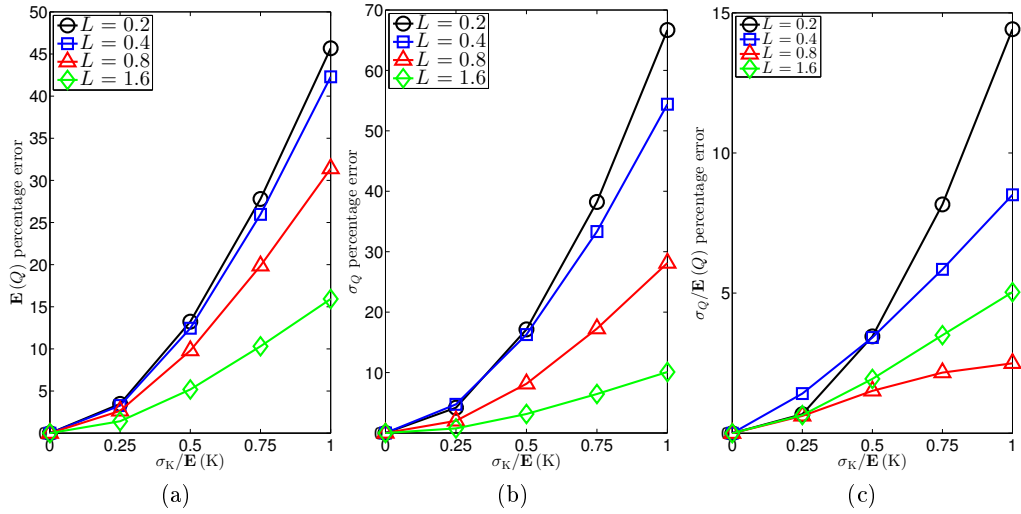


Figure 9: Plots of percentage differences between nonlinear and linear estimates for (a) the mean flux $\mathbb{E}(Q)$; (b) the standard deviation of the flux σ_Q and (c) the ratio $\sigma_Q/\mathbb{E}(Q)$ of the mean and standard deviation of the flux as functions of normalised permeability standard deviation $\sigma_K/\mathbb{E}(K)$. Values plotted for correlation length scales $L = 0.2$ (black with circles), $L = 0.4$ (blue with squares), $L = 0.8$ (red with triangles) and $L = 1.6$ (green with diamonds).

as the standard deviation of the permeability fields increases. The differences between the estimates also increase as the correlation length L decreases for both the mean and the standard deviation of the flux. We interpret this effect as being a consequence of the fact that for small correlation length scales there are more permeability fluctuations in series along a flow streamline. The nonlinear calculation for the flux accounts for the geometric averaging of the permeability along the streamline while the linear estimate only takes the arithmetic mean.

Figures 9a and 9b show that as the standard deviation of the permeability increases beyond 0.5 we see significant differences between the linear estimates and the nonlinear values for the statistics of the flux. However the linear estimates and nonlinear calculations for the fractional uncertainty of the flux $\sigma_Q/\mathbb{E}(Q)$ are in good agreement as shown in figure 9c. We again observe an increase in the difference as σ_K increases. However, even for $L = 0.2$ and $\sigma_K/\mathbb{E}(K) = 1$ the error is less than 15%. This is due to cancellation of the errors shown in figures 9a and 9b. The linear estimates for the mean and the standard deviation are both higher than the nonlinear estimates and hence we see the reduced error in figure 9c. However we encourage caution when applying the linear estimates for standard deviations of permeability above 0.5 as the differences between nonlinear and linear values for the mean and standard deviation of the flux are large.

7. Kriging

Kriging was first proposed as an interpolation method by D. G. Krige (Krige 1951) and subsequently promoted and developed by G. Matheron (Matheron 1971). It is described as the ‘‘Best Linear Unbiased Estimator’’ (‘B.L.U.E.’) where ‘Best’ means that this technique gives the linear estimator with the minimal error variance whilst remaining unbiased. The extent to which kriging is the best interpolation method to use in any given situation is beyond the scope of this paper. We use kriging merely as an example of a widely used linear interpolation method. The strategies employed below can be similarly applied to any linear regression model used to estimate the permeability.

Kriging is a linear interpolation method used to estimate the permeability K at point \mathbf{x}_0 given the values of the permeability at sample points \mathbf{x}_i . The estimate $K(\mathbf{x}_0)$ is taken as a linear combination of the sampled values $K(\mathbf{x}_i)$ with weights w_i ,

$$K(\mathbf{x}_0) = \sum_i w_i K(\mathbf{x}_i). \quad (7.1)$$

The weightings in (7.1) are given by the ordinary kriging equations

$$M\mathbf{w} = \begin{pmatrix} C_{11} & \dots & C_{1n} & 1 \\ \vdots & \ddots & \vdots & \vdots \\ C_{n1} & \dots & C_{nn} & 1 \\ 1 & \dots & 1 & 0 \end{pmatrix} \begin{pmatrix} w_1 \\ \vdots \\ w_n \\ \lambda \end{pmatrix} = \begin{pmatrix} C_{01} \\ \vdots \\ C_{0n} \\ 1 \end{pmatrix} = \mathbf{c}, \quad (7.2)$$

where λ is a lagrange multiplier and $C_{ij} = \text{Cov}(\mathbf{x}_i, \mathbf{x}_j)$ is the covariance of the permeability at the pair of points $\mathbf{x}_i, \mathbf{x}_j$. The covariances C_{ij} will depend upon the correlation length scale L of the covariance model. To calculate the sensitivity of the flux Q to changing the correlation length scale L we can calculate the derivative $\frac{dQ}{dL}$, which by (3.3) is given by

$$\frac{\partial Q}{\partial L} = \frac{1}{\Delta p} \int_{\mathcal{D}} (\nabla p)^\top \frac{\partial K}{\partial L} \nabla p \, dV. \quad (7.3)$$

Further, $\frac{\partial K}{\partial L}$ is given by

$$\frac{\partial K}{\partial L} = \sum_i \frac{dw_i}{dL} K(\mathbf{x}_i), \quad (7.4)$$

where $\frac{dw_i}{dL}$ can be estimated by perturbing L and recalculating w_i or can be found directly through use of

$$\frac{\partial \mathbf{w}}{\partial L} = M^{-1} \frac{\partial \mathbf{c}}{\partial L} + \frac{\partial}{\partial L} (M^{-1}) \mathbf{c} = M^{-1} \left(\frac{\partial \mathbf{c}}{\partial L} - \frac{\partial M}{\partial L} M^{-1} \mathbf{c} \right). \quad (7.5)$$

To derive (7.5) we have used the identity

$$\frac{dM^{-1}}{dL} = -M^{-1} \frac{dM}{dL} M^{-1}, \quad (7.6)$$

for the derivative of a matrix inverse. Use of (7.6) allows us to calculate the derivative of M^{-1} without calculating M^{-1} symbolically. To demonstrate the use of these results in practice we shall use the permeability field shown in figure 6a as a surrogate truth model. For the field shown in figure 6a we have set the minimum permeability equal to machine precision above zero and specified a standard deviation equal to 1. This choice of this value for the minimum permeability was selected so as to give a large range of permeabilities compared with the minimum permeability value. This should yield a demanding test for our linear methods.

In practice the true permeability field is not usually known and to estimate the permeability one must interpolate from a limited amount of sampled points. We will suppose we have measured the permeability at fixed locations from which we will estimate the permeability through kriging. Given the permeability data at the sample locations, the correlation length scale can be estimated using the maximum likelihood estimator

$$L^* = \min_L \left(\psi(L) \equiv |R|^{\frac{1}{n}} \sigma^2 \right), \quad (7.7)$$

where n is the number of sample locations, $|R|$ is the determinant of the matrix of covariances (that is $(R)_{ij} = C_{ij}$) and σ^2 is the process variance given by

$$\sigma^2 = \frac{1}{n} (\mathbf{Y} - \mathbf{F}\beta^*)^\top R^{-1} (\mathbf{Y} - \mathbf{F}\beta^*), \quad (7.8)$$

where \mathbf{Y} is the vector of permeability values at the sample locations and $\mathbf{F}^\top = (1, \dots, 1)$ with β^* given by

$$\beta^* = (\mathbf{F}^\top R^{-1} \mathbf{F})^{-1} \mathbf{F}^\top R^{-1} \mathbf{Y}. \quad (7.9)$$

(See Lophaven, Nielsen & Søndergaard (2002) for a more thorough discussion of this maximum likelihood estimation). For this example we have $m = 16$ sample locations with one at each of the source ($x = (-0.5, 0)$) and sink ($x = (0.5, 0)$) and the remaining fourteen randomly located throughout the 4 by 4 flow domain. The sample locations are shown by the black dots in figures 10a and 10b. With these locations and associated permeability data the maximum likelihood estimate of the correlation length is $L^* = 0.3953$, which is very close to the correlation length scale of 0.4 used in the surrogate permeability (figure 6a). For this length scale and a gaussian correlation function the kriged permeability field is shown in figure 10a. This estimation conserves some of the features of the surrogate permeability field, though due to the limitations of kriging and interpolation in general, many of the features are lost. Notably, the range of permeabilities has been reduced from approximately $[0, 5]$ to approximately $[1.5, 4]$. Although it is noteworthy that this loss of information is likely to influence the estimated flow quantities, the

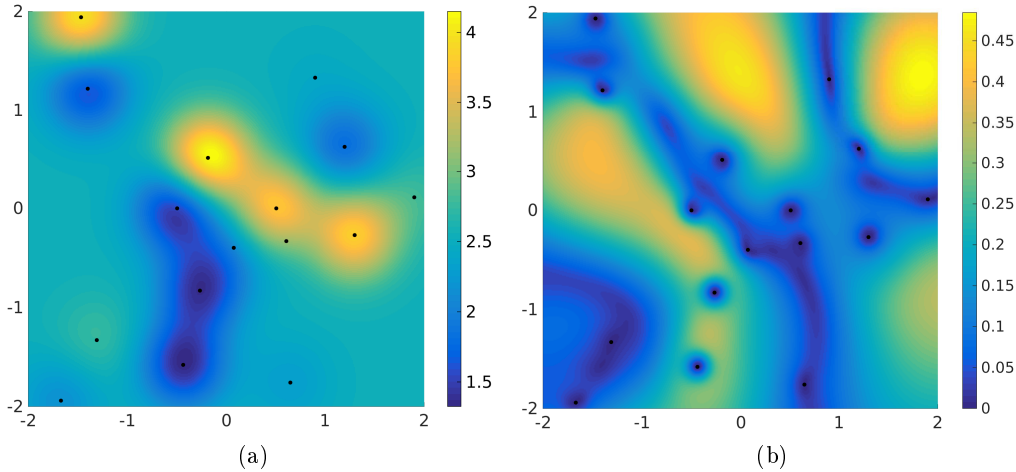


Figure 10: (a) Kriged permeability estimated from (7.1) and (7.2) with correlation length scale $L^* = 0.3953$. (b) Standard deviation of permeability as a fraction of the base field (shown in (a)) as a function of location as the correlation length scale is varied across $(L^*/4, 4L^*)$. Data sample locations shown by black dots.

failings of interpolation to characterise the surrogate permeability fully are not the focus of this paper.

To analyse the sensitivity of the flux to changes in correlation length we vary the correlation length across 1001 values across $[L^*/4, 4L^*]$. For each value we calculate the associated kriged permeability field. Figure 10b shows the standard deviation of the permeability normalised by the permeability values given in figure 10a. That is, figure 10b shows by how much the permeability varies as the correlation length scale is varied. To apply the techniques detailed in §3 and §4 we hope for the standard deviation to be small relative to the mean which in figure 10b corresponds to values which are small compared with 1. We can expect a significant error when estimating the flux if there are locations in the domain where the permeability values have standard deviation approaching or greater than 1, especially if this occurs in close proximity to the source or the sink where the pressure gradients are highest. Figure 10b shows that the standard deviation of the permeability is less than the value of the reference permeability across the domain. Most of the domain shows a deviation of around or below 0.4 with a couple of locations with higher variability. From this diagnostic figure we can predict that the error in our linear flux estimates will be small given that the locations of high variability are towards the edges of the flow domain where we expect lower pressure gradients.

The nonlinear approach to calculating the flux for each sample of the permeability field requires calculation of the pressure field from (2.2) for each permeability realisation. However, using (4.10) we can gain an estimate for the flux resulting from each different permeability with only one pressure calculation, similarly to §4. The nonlinear results are shown in figure 11a by the black dashed line while the linear estimate is shown by the blue full line. We have restricted the maximum value of the x-axis as for higher correlation length scales some areas of the permeability field become negative. This is both unphysical and changes the equation for the pressure field

$$\nabla \cdot (K \nabla p) = 0, \quad (7.10)$$

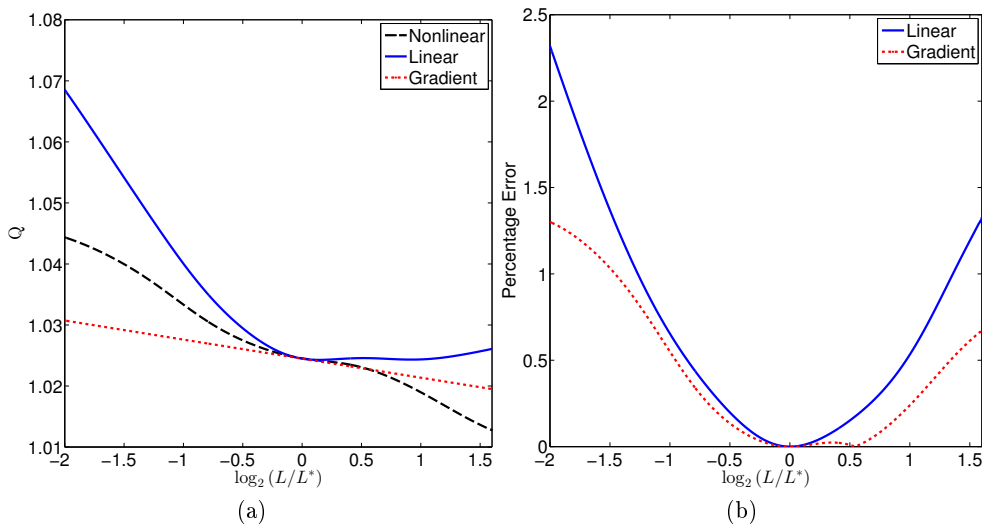


Figure 11: (a) Predicted flux against kriging correlation length scale (shown on log scale) from fully nonlinear calculations (black dashed line), linear flux calculation (blue full line) and flux gradient calculation (red dotted line). (b) Percentage difference between nonlinear calculation and linear flux (blue full line) and flux gradient (red dotted line) against kriging correlation length scale (shown on log scale).

from an elliptic equation to a locally hyperbolic equation resulting in an ill-posed problem.

We can also gain an estimate for the change in flux with respect to correlation length through the use of the gradient given by (7.3), (7.4) and (7.5). This is shown by the red dotted line in figure 11a. As expected, the linear and gradient estimates both agree with the nonlinear result for $L = L^*$ and the blue full line lies entirely above the black dashed line, consistent with the fact that the second order error term (4.9b) for the flux is negative. That is, the linear estimate for the flux is an upper bound for the value of the nonlinear flux. Figure 11b shows the percentage difference between the two estimates used and the nonlinear values for the flux. Encouragingly, this difference is below 2.5% even for a factor of four change in the correlation length scale. In this example the gradient estimate agrees more closely with the nonlinear calculation though this is not observed to be a general trend.

8. Imposing positive permeability

An issue that arises when using kriging is that the kriging method does not include any constraint on the resulting estimated values. When estimating a positive quantity such as permeability this can lead to negative or otherwise unphysical values as observed in §7. There are several techniques that have been proposed to impose positivity constraints on the estimated values. Some involve removing negative weights after solving the ordinary kriging equations (7.2) (see, for example, Deutsch (1996)). A technique developed by Kostov & Dubrule (1986) incorporates the constraints on the values to be estimated within the interpolation procedure. The permeability at the location of the estimate is written as

$$K(\mathbf{x}_0) = \bar{K} + \sum_i b_i C_{0i}, \quad (8.1)$$

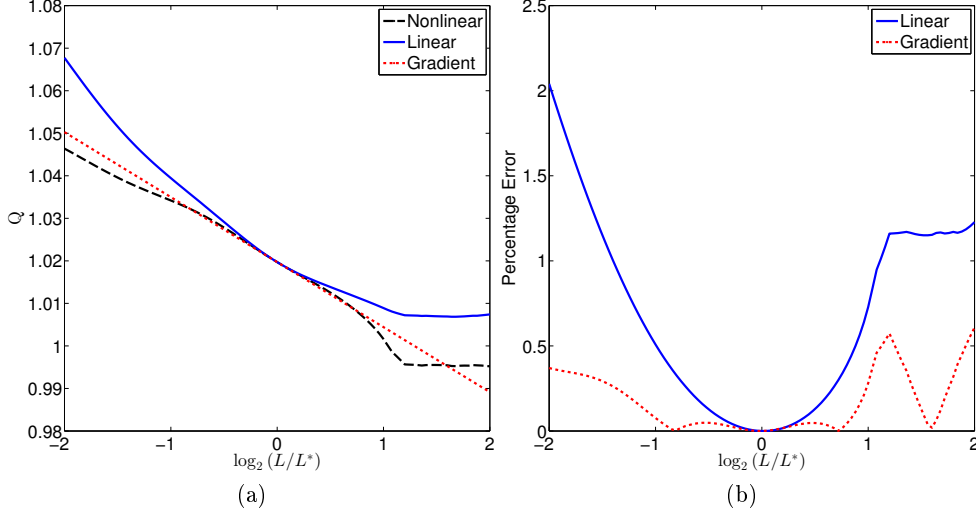


Figure 12: (a) Predicted flux against correlation length scale (shown on log scale) from fully nonlinear calculations (black dashed line), linear flux calculation (blue full line) and flux gradient calculation (red dotted line). (b) Percentage difference between nonlinear calculations and linear flux (blue full line) and flux gradient (red dotted line) against correlation length scale (shown on log scale).

where the weights b_i are to be determined and where \bar{K} is a trend model which we take here to be the mean value of the sampled permeability data. We impose the following constraints

$$K(\mathbf{x}_i) = k_i \quad \text{for } 1 \leq i \leq n, \quad (8.2a)$$

$$K(\mathbf{x}_i) \geq 0 \quad \text{for } n+1 \leq i \leq n+m, \quad (8.2b)$$

where k_i is the sampled value of the permeability at the sample location \mathbf{x}_i , n is the number of sample locations and m is the number of points at which we wish to estimate the permeability. Kostov & Dubrule (1986) propose that the weights b_i in (8.1) can be taken as the solution to

$$\min_{\mathbf{b}} f(\mathbf{b}; L) = \min_{\mathbf{b}} (\mathbf{b}^T R \mathbf{b} - \mathbf{B}^T \mathbf{b}), \quad (8.3a)$$

$$b_i \geq 0 \quad \text{for } n+1 \leq i \leq n+m, \quad (8.3b)$$

where $\mathbf{b} = (b_1, \dots, b_{n+m})$ and $\mathbf{B}^T = (K_1, \dots, K_n, 0, \dots, 0)$. One justification for the form of (8.3a) is the equivalence with the kriging equations (7.2) when the positivity constraints (8.2b) are removed. The gradient of the flux $\frac{dQ}{dL}$ given by (7.3) can again be calculated for this interpolation technique through use of

$$\frac{\partial K}{\partial L} = \sum_i \frac{\partial b_i}{\partial L} \text{Cov}(\mathbf{x}_0, \mathbf{x}_i) + b_i \frac{\partial}{\partial L} (\text{Cov}(\mathbf{x}_0, \mathbf{x}_i)). \quad (8.4)$$

By defining $f = \mathbf{b}^T R \mathbf{b} - \mathbf{B}^T \mathbf{b}$ we can calculate $\frac{\partial b_i}{\partial L}$ by noting that the change in the minimum of f will be given by

$$\frac{\partial \mathbf{b}}{\partial L} = -\nabla \left(\frac{\partial f}{\partial L} \right), \quad (8.5)$$

where the ∇ operator is with respect to \mathbf{b} .

Similarly to §7 we vary the correlation length across 101 values within $(L^*/4, 4L^*)$. The reduction in the number of simulations in comparison to §7 is due to the increased computation time for each realisation of the permeability. The results of the nonlinear (black dashed line), linear (blue full line) and gradient (red dotted line) estimates for the flux are shown in figure 12a and the percentage differences between the linear (blue full line)/gradient (red dotted line) and the nonlinear values are shown in figure 12b. Once again the linear and gradient estimates agree well with the nonlinear flux values. The flattened behaviour in figure 12a of the nonlinear and linear flux values for large values of correlation length scales L arises when the positivity constraints (8.2a) impose a different permeability estimate to that which would be attained by the kriging equations (7.2).

9. Conclusions

We have presented a derivation of an integral expression for the total flux of a single phase incompressible fluid through a porous medium. Taking variations of this expression with respect to parameters which describe the permeability field results in an integral relationship between the derivative of the flux and the derivative of the permeability. This can then be used to calculate directly the sensitivity of the flux to the individual parameters of the permeability model. Through a simplified example we have shown that this sensitivity is dependent upon the position of the source and sink relative to the geological structure captured in the permeability model. We have restricted ourselves to single phase flow. For multiphase flow we can use the same method provided the location of the various different fluids is known or, more precisely, the viscosity is known as a function of space. In this case we replace K by K/μ . However, without knowledge of the front location, this problem cannot currently be approached with the methods of this paper.

The use of a perturbation expansion has allowed us to approximate the exact expression for the flux with another integral expression which is independent of pressure changes induced by a change in the permeability field. By representing each discrete value by an independent random variable we are able to derive a relationship between the statistical moments of the permeability and those of the flux. This relationship can then be used to estimate the number of permeability parameters which should be varied in a nonlinear calculation for the variance of the flux. When compared to nonlinear calculations there is good agreement for changes in permeability which are small compared to the base permeability. Indeed, in the sample flow geometry considered here the agreement remains reasonable as the change in permeability becomes the same size as the base permeability. In principle, it is possible to construct a power series expansion for the flux as a function of the permeability parameters, improving the accuracy of the estimates given here.

To assess the applicability of the linear methods to more complex permeability fields we have considered several further methods of permeability modelling. For spectral methods and other ways of generating stochastic realisations we cannot directly compute derivatives though we may use the linear estimation process to calculate the flux for each realisation of the permeability. For 1000 realisation sample sets of permeability fields we found that the linear estimates are in good agreement with nonlinear calculations for the majority of permeability realisations when the standard deviation of the permeability fields is sufficiently small. Also the linearly estimated statistics of the flux show good agreement with the nonlinear values. We have further shown that, when linear interpolation methods are used to generate permeability fields, we can apply the linear methods to assess the sensitivity of the flux to changes in the model interpolation parameters used.

For the examples given the linear estimates show remarkably good agreement to the nonlinear results derived through repeated direct calculation of the flux for each realisation of the permeability. It is interesting that the error of the linear estimates compared to nonlinear calculations are small for the layered and interpolation examples. For the layered example this is because the permeability values have a long correlation length scale in the macroscopic direction of the flow. Hence the arithmetic average of the permeabilities which the linear estimate implicitly calculates is appropriate. The errors between nonlinear and linear estimates for interpolated permeability fields are small because the permeability is constrained in areas of the domain where pressure gradients are high. By contrast the stochastic examples of §6 show that when there are unconstrained fluctuations in permeability at small correlation length scales, the error of the linear estimate is large.

The derived expressions for the derivatives of the flux with respect to the permeability parameters and for the linearised flux changes are independent of changes in the pressure field resulting from changes in the permeability. We have exploited this independence throughout the paper to reduce significantly the number of flow calculations required compared to a Monte Carlo approach. The linearised method presented in §4 becomes invalid as the magnitude of the variations in permeability away from the leading order value become large. Nevertheless, for sufficiently small permeability variations our method obviates the need for a flow calculation for each realisation of the permeability sampled from a probability distribution of possibilities. This enables a fast characterisation of the sensitivity of the flux estimate to the parameters of the permeability model and allows us to calculate average values with a minimal number of flow calculations. This insight can then be used, for example, to inform a more precise or detailed flow model.

The support of an Industrial CASE studentship from EPSRC and BP for A. J. Evans entitled "Optimal Reservoir Modelling" is gratefully acknowledged.

REFERENCES

- BEAR, J. 1972 *Dynamics of Fluids in Porous Media*. Dover.
- BLACK, T. C. & FREYBERG, D. L. 1990 Simulation of one-dimensional correlated fields using a matrix-factorization moving average approach, *Mathematical Geology*, 22(1), 39-62.
- BORGMAN, L., TAHERI, M. AND HAGAN, R. 1984 Three-dimensional frequency-domain simulations of geological variables, *Geostatistics for Natural Resource Characterization*, edited by G. Verly, M. David, A. G. Journel, and A. Marechal, pp. 517-541.
- CHILÉS, J. P. & DELFINER, P. 1999 *Geostatistics: Modeling Spatial Uncertainty*. Wiley: New York.
- CHRISTIE, M. A. 1996 Upscaling for Reservoir Simulation. *Journal of Petroleum Technology*, 48(11):1004-1010.
- CUSHMAN, J. H., BENNETHUM, L. S. & HU, B. X. 2002 A primer on upscaling tools for porous media. *Advances in Water Resources*, Vol 25, pp. 1043-1067.
- DAVIS, M. W. 1987 Production of conditional simulations via the LU triangular decomposition of the covariance matrix, *Mathematical Geology*, 19(2), 91-98.
- DESBARATS, A. J. 1992 Spatial averaging of hydraulic conductivity in three-dimensional heterogeneous porous media, *Mathematical Geology*, 24(3), 249-267.
- DEUTSCH, C. V. 1996 Correcting for negative weights in ordinary kriging, *Computers & Geosciences*, 22(7), pp. 765-773.
- DIETRICH, C. R. & NEWSAM G. N. 1993 A Fast and Exact Method for Multidimensional Gaussian Stochastic Simulations *Water Resources Research*, Vol 29, No. 8, pp. 2861-2869.
- FARMER, C. L. 2002 Upscaling: a review. *Int. J. Numer. Meth. Fluids*, 40:63-78.
- FIORI, A., DAGAN, G. & JANKOVIC, I. 2013 Upscaling of flow in heterogeneous porous forma-

- tions: Critical examination and issues of principle. *Advances in Water Resources*, Vol 51, pp. 67-85.
- JAHN, F., COOK, M. & GRAHAM, M. 2008 Hydrocarbon Exploration & Production. *Elsevier*, Chap. 14.
- GAVALAS, G.R., SHAH, P.C. & SEINFELD, J.H. 1976 Reservoir history matching by Bayesian estimation. *SPE Journal*, Vol 16, No 6.
- GERRITSEN, M. G. & DURLOFSKY, L. J. 2005 Modeling Fluid Flow in Oil Reservoirs. *Annu. Rev. Fluid Mech*, 37:211-38.
- KING, M. J., KING, P.R., MCGILL, C. A. & WILLIAMS, J. K. 1995 Effective properties for flow calculations. *Transport in Porous Media*, 20:169-196.
- KING, P. R. & SMITH, P. J. 1988 Generation of correlated properties in heterogeneous porous media, *Mathematical Geology*, 20(7), 863-877.
- KOSTOV, C. & DUBRULE, O. 1986 An Interpolation Method Taking into Account Inequality Constraints: II. Practical Approach, *Mathematical Geology*, Vol. 18, No. 1.
- KRIGE, D. G. 1951 A statistical approach to some basic mine valuation problems on the Witwatersrand, *Journal of the Chem., Metal. and Mining Soc. of South Africa* 52 (6): 119-139.
- MANTOGLOU, A. & WILSON, J. L. 1982 The turning bands methods for simulation of random fields using line generation by a spectral method, *Water Resources Research*, 18(5), 1379-1394.
- MATHERON G. 1971 The Theory of Regionalized Variables and its Applications, *Les Cahiers du Centre de Morphologie Mathématique de Fontainebleu No 5*, Ecole Nationale Supérieure de Mines de Paris.
- LOPHAVEN, S. N., NIELSEN, H. B., & SØNDERGAARD, J. 2002 DACE a matlab kriging toolbox. *Informatics and Mathematical Modelling*, IMM-TR-2002-12.
- RENARD PH. & DE MARSILY, G. 1997 Calculating equivalent permeability: a review. *Advances in Water Resources*, Vol 20, Nos 5-6, pp. 253-278.
- WEN, X. & GÓMEZ-HERNÁNDEZ, J. 1996 Upscaling hydraulic conductivities in heterogeneous media: An overview. *Journal of Hydrology*, Vol 183.
- WU, X. H., EFENDIEV, Y. & HOU, T. Y. 2002 Analysis of Upscaling Absolute Permeability. *Discrete and Continuous Dynamical Systems - Series B*, Volume 2, Number 2.
- YILMAZ, Ö. 2001 Seismic Data Analysis: Processing, Inversion, and Interpretation of Seismic Data, Volume 2 *SEG Books*.